

# Optical conductivity of nodal metals

C. C. Homes,<sup>1,\*</sup> J. J. Tu,<sup>2,†</sup> J. Li,<sup>2</sup> G. D. Gu,<sup>1</sup> and A. Akrap<sup>3</sup>

<sup>1</sup>*Condensed Matter Physics and Materials Science Department,  
Brookhaven National Laboratory, Upton, New York 11973, USA*

<sup>2</sup>*Department of Physics, The City College of New York, New York, New York 10031, USA*

<sup>3</sup>*École de Physique, Université de Genève, CH-1211 Genève 4, Switzerland*

(Dated: August 17, 2018)

Fermi liquid theory is remarkably successful in describing the transport and optical properties of metals; at frequencies higher than the scattering rate, the optical conductivity adopts the well-known power law behavior  $\sigma_1(\omega) \propto \omega^{-2}$ . We have observed an unusual non-Fermi liquid response  $\sigma_1(\omega) \propto \omega^{-1\pm 0.2}$  in the ground states of several cuprate and iron-based materials which undergo electronic or magnetic phase transitions resulting in dramatically reduced or nodal Fermi surfaces. The identification of an inverse (or fractional) power-law behavior in the residual optical conductivity now permits the removal of this contribution, revealing the direct transitions across the gap and allowing the nature of the electron-boson coupling to be probed. The non-Fermi liquid behavior in these systems may be the result of a common Fermi surface topology of Dirac cone-like features in the electronic dispersion.

In a Fermi liquid, the complex conductivity  $\tilde{\sigma} = \sigma_1 + i\sigma_2$  can be expressed through the generalized Drude model,  $\tilde{\sigma}(\omega) = (\omega_p^2/60) / \{1/\tau(\omega) - i\omega [1 + \lambda(\omega)]\}$  (in units of  $\Omega^{-1}\text{cm}^{-1}$ ), where  $\omega_p^2 = 4\pi n e^2/m_b$ ,  $1/\tau(\omega)$  and  $1 + \lambda(\omega) = m^*(\omega)/m_b$  are the plasma frequency, frequency-dependent scattering rate and mass enhancement, respectively, where  $n$  is a carrier concentration and  $m_b$  is the band mass. At low-temperature the scattering rate will vary quadratically with frequency and temperature,  $1/\tau(\omega, T) = 1/\tau_0 + A [(\hbar\omega)^2 + (2\pi k_B T)^2]$ , where  $A$  is a constant that varies with the material [1, 2]. In the frequency domain, for  $\omega\tau \ll 1$  the conductivity varies slowly, but for  $\omega\tau \gg 1$  the conductivity adopts a power-law behavior,  $\sigma_1 \propto \omega^{-2}$ ; however, deviations from this behavior may be observed in strongly-correlated electronic systems [3–7].

## RESULTS

The temperature dependence of the optical conductivity of optimally-doped  $\text{Bi}_2\text{Sr}_2\text{CaCu}_2\text{O}_{8+\delta}$ , one of the most thoroughly studied cuprate high-temperature superconductors [8], is shown versus wave number (photon energy) in a log-log plot in Fig. 1a for light polarized along the crystallographic  $a$  axis [9]. Just above  $T_c$  it may be argued that the optical properties are consistent with those of a Fermi liquid (see Supplementary Information and Fig. S1 online for a discussion of different models for the optical conductivity and the frequency-dependent scattering rate); this statement is in keeping with the proposed phase diagram for the high-temperature superconductors [10]. Below  $T_c$  there is a rapid reduction of the low-frequency conductivity or spectral weight, which is defined as the area under the conductivity curve; this ‘missing spectral weight’ is the optical signature for the formation of a superconducting condensate [8]. However,

even down to the lowest measured temperature there is still a significant amount of low-frequency residual conductivity [11]. This is because, unlike a conventional  $s$ -wave superconductor in which the entire Fermi surface is completely gapped below  $T_c$ , the cuprate materials have a momentum-dependent  $d$ -wave gap that contains nodes [12, 13],  $\Delta(\mathbf{k}) = \Delta_0 [\cos(k_x a) - \cos(k_y a)]$ , where  $\Delta_0$  is the gap maximum.

The presence of nodes allows pair-breaking out of the superconducting state resulting in unpaired nodal quasiparticles [14]. For low photon energies ( $\hbar\omega \ll 2\Delta_0$ ) only the nodal structure of the  $d$ -wave gap is probed and the Fermi surface topology is similar to that of the Dirac cone observed in graphene and other quantum materials [15, 16]. The rapid collapse of the quasiparticle scattering rate [17] below  $T_c$  indicates that in the far-infrared region  $\omega\tau \gg 1$ , so  $\sigma_1 \propto \omega^{-2}$  should be clearly revealed. Surprisingly, what is observed instead is that below  $T_c$  low-frequency residual optical conductivity forms a family of lines with the same non-Fermi liquid fractional power law behavior  $\sigma_1 \propto \omega^{-1.2}$ ; in metallic systems at low-frequency where  $\sigma_1 \gg \sigma_2$ , this is approximately equivalent to the scattering rate having a fractional power law behavior  $1/\tau \propto \omega^{1.2}$ . Another family of cuprates that has been extensively investigated are the  $\text{YBa}_2\text{Cu}_3\text{O}_{6+y}$  materials. The optical conductivity of optimally-doped  $\text{YBa}_2\text{Cu}_3\text{O}_{6.95}$  is shown in Fig. 1b for light polarized along the  $a$  axis; this crystallographic axis is transverse to the copper-oxygen chains and should therefore probe the dynamics of only the copper-oxygen planes [18]. Well below  $T_c$ , the observed power law for the residual conductivity  $\sigma_1 \propto \omega^{-1.2}$  is identical to the response observed in optimally-doped  $\text{Bi}_2\text{Sr}_2\text{CaCu}_2\text{O}_{8+\delta}$ . The underdoped  $\text{YBa}_2\text{Cu}_3\text{O}_{6.60}$  sample is of particular interest due to the formation of a pseudogap in the normal state [19] and the commensurate reduction of the Fermi surface around the nodal regions, a condition that has been referred to

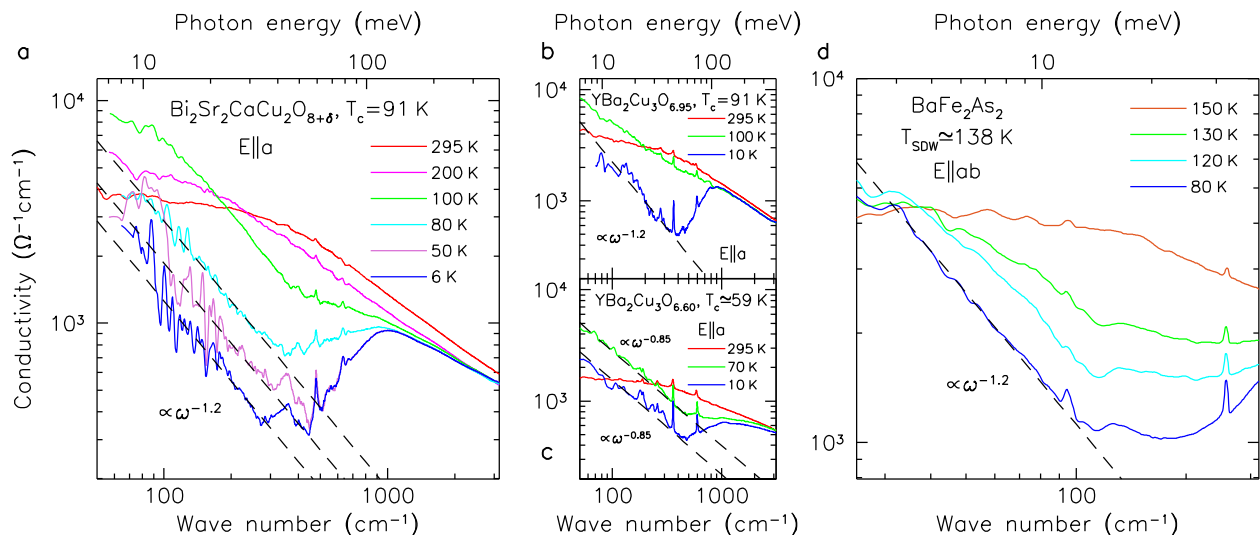


**Figure 1 | The optical conductivity of some quantum materials.** **a**, The temperature dependence of the optical conductivity versus wave number (photon energy) for optimally-doped  $\text{Bi}_2\text{Sr}_2\text{CaCu}_2\text{O}_{8+\delta}$  ( $T_c = 91$  K) for light polarized along the crystallographic  $a$  axis. At low frequency just above  $T_c$  the material may be cautiously described as a Fermi liquid. For all the temperatures measured below  $T_c$  the residual conductivity from the unpaired quasiparticles follows the same non-Fermi liquid fractional power law,  $\sigma_1(\omega) \propto \omega^{-1.2}$ . **b**, The plot for optimally-doped  $\text{YBa}_2\text{Cu}_3\text{O}_{6.95}$  ( $T_c = 91$  K), for light polarized along the  $a$  axis, illustrating the fractional power law below  $T_c$ . **c**, The plot for underdoped  $\text{YBa}_2\text{Cu}_3\text{O}_{6.60}$  ( $T_c \simeq 59$  K), for light polarized along the  $a$  axis, illustrating an identical (non-Fermi liquid) fractional power-law behavior in the normal (pseudogap) and superconducting states. **d**, The plot for the  $\text{BaFe}_2\text{As}_2$  ( $T_{\text{SDW}} = 138$  K), for light polarized in the  $a$ - $b$  planes. Below  $T_{\text{SDW}}$  the fractional power law  $\sigma_1 \propto \omega^{-1.2}$  is again observed.

as a ‘nodal metal’ [20, 21]. The optical conductivity for this material is shown in Fig. 1c for light polarized along the  $a$  axis. Just above  $T_c$  in the normal state the low-frequency optical conductivity may be described using a non-Fermi liquid power-law,  $\sigma_1 \propto \omega^{-0.85}$ ; however, what is fascinating is that well below  $T_c$  the response of the unpaired quasiparticles displays the identical fractional power law. This indicates the (unpaired) quasiparticles appear to behave the same way regardless of whether it is the pseudogap that results in the reduction of a large Fermi surface to a small arc or pocket [22], or the formation of a  $d$ -wave superconducting energy gap resulting in nodes. This non-Fermi liquid power-law behavior in the underdoped material has been previously observed in the microwave region [23]; however, in that work the exponent is considerably larger,  $\sigma_1 \propto \omega^{-1.45}$ . The most likely source for this disagreement is the fact that the microwave experiments are done in the  $\omega\tau \sim 1$  region, while the optical work was performed in the  $\omega\tau \gg 1$  limit, suggesting that the relaxation processes in these two regimes may be different. Surprisingly, recent results on the single-layer, underdoped cuprate  $\text{HgBa}_2\text{CuO}_{4+\delta}$  demonstrate that it displays Fermi liquid-like behavior [24], indicating that the nature of the underdoped (pseudogap) region in the cuprate materials is still controversial.

Interestingly, an almost identical behavior has also been observed in the  $A\text{Fe}_2\text{As}_2$  ( $A = \text{Ba}$  and  $\text{Ca}$ ) iron-

arsenic compounds [25]. In  $\text{BaFe}_2\text{As}_2$  a spin-density-wave (SDW) state develops below  $T_{\text{SDW}} \simeq 138$  K, resulting in the formation of a Dirac-like cone in the electronic dispersion close to the Fermi surface [26, 27] with small pockets or puddles. The frequency-dependent scattering rate has a clear quadratic component just above  $T_{\text{SDW}}$ , suggesting the non-magnetic state of this material may be described as a Fermi liquid (see Supplementary Fig. S2a online); when the SDW transition is removed by Co substitution, the quadratic behavior persists from 295 K down to 27 K (see Supplementary Fig. S2b online). The optical conductivity of  $\text{BaFe}_2\text{As}_2$  is shown in Fig. 1d; for  $T \ll T_{\text{SDW}}$  we once again observe the fractional power law in the residual low-frequency optical conductivity [28],  $\sigma_1 \propto \omega^{-1.2}$ , similar to that seen in the ground state of several of the cuprates. The identical power law is also observed in  $\text{CaFe}_2\text{As}_2$  for  $T \ll T_{\text{SDW}}$  (see Supplementary Fig. S3 online).

## DISCUSSION

One important aspect of the fractional power law lies in its ability to remove the nodal quasiparticle (residual) response that masks the gap. In a superconductor, the real part of the optical conductivity at low frequencies may be expressed as the linear combination  $\sigma_1(\omega) = \delta(0) + \sigma_{\text{qp}} + \sigma_{\text{gap}} + \dots$ , where  $\delta(0)$  is the zero-

frequency component that corresponds to the superfluid density,  $\sigma_{\text{qp}}$  is the conductivity due to the unpaired quasiparticles, and  $\sigma_{\text{gap}}$  is the contribution due to direct excitations across the gap. [In the normal state,  $\delta(0)$  is absent and  $\sigma_{\text{qp}}$  is just the quasiparticle response from the whole Fermi surface.] Because we now have an explicit functional form for  $\sigma_{\text{qp}}$  for various materials, then for  $\omega > 0$  we neglect  $\delta(0)$  and the low-frequency response is  $\sigma_{\text{gap}} \simeq \sigma_1(\omega) - \sigma_{\text{qp}}$ . The conductivity due to the superconducting energy gap may be described phenomenologically using a Kubo-Greenwood approach [29] in which all the zero-momentum transitions across the gap in the Brillouin zone are considered; in general terms, the optical conductivity due to the gap is a reflection of the joint density of states of the photo-excited electron and hole pairs. In a conventional superconductor with an isotropic energy gap  $\Delta$  and weak coupling to phonons (or any other exchange boson), then for  $T \ll T_c$  in systems at or close to the dirty limit [ $1/\tau_0 \gtrsim 2\Delta$  where  $1/\tau_0 = 1/\tau(\omega \rightarrow 0)$ ], the onset of absorption will occur at  $2\Delta$ ; for modest coupling, this onset shifts to  $\Omega_0 + 2\Delta$ , where  $\Omega_0$  is the energy of the boson [30, 31]. Similarly, in a  $d$ -wave superconductor in the dirty limit with weak coupling, the onset would be expected at  $\omega \simeq 0$ ; however, for moderate coupling the onset should shift to  $\Omega_0$  with a local maximum at  $\simeq \Omega_0 + 2\Delta_0$ .

The result for the removal of the quasiparticle contribution,  $\sigma_1(\omega) - \sigma_{\text{qp}}$ , is shown in Fig. 2 for  $\text{Bi}_2\text{Sr}_2\text{CaCu}_2\text{O}_{8+\delta}$  at  $\sim 6$  K, well below  $T_c$  the resulting conductivity is effectively zero at low frequency and the onset of conductivity does not begin until  $\omega \gtrsim 400 \text{ cm}^{-1}$ . This corresponds to the bosonic excitation at  $\Omega_0$ , the frequency above which a change occurs in the optical conductivity due to the strong renormalization of the scattering rate (see Fig. 1a). This indicates that there is at least moderate electron-boson coupling in this material [32, 33] and that the local maximum in the conductivity will be at  $\simeq \Omega_0 + 2\Delta_0$ . The inferred values of  $\Omega_0 \simeq 50 \text{ meV}$  and  $\Delta_0 \simeq 35 \text{ meV}$  are in good agreement with estimates for these quantities based from angle-resolved photoemission spectroscopy [13], and are consistent with optical inversion techniques [9, 34]. This procedure may also be successfully applied to the  $\text{YBa}_2\text{Cu}_3\text{O}_{6+y}$  materials (see Supplementary Fig. S4 online), as well as the iron-based  $\text{BaFe}_2\text{As}_2$  and  $\text{CaFe}_2\text{As}_2$  materials in their SDW states (see Supplementary Fig. S5 online).

The significance of our finding is the common fractional power law behavior of the low-frequency optical conductivity (THz and far-infrared regions) in materials with Dirac cone-like electronic dispersion and nodal Fermi surfaces. More generally, the fractional power law behavior signals the importance of many-body effects in quantum materials with this unique electronic dispersion, where the fractional power law in conductivity is roughly equivalent to a nearly-linear frequency dependence of the scattering rate. Similar results have been found in single

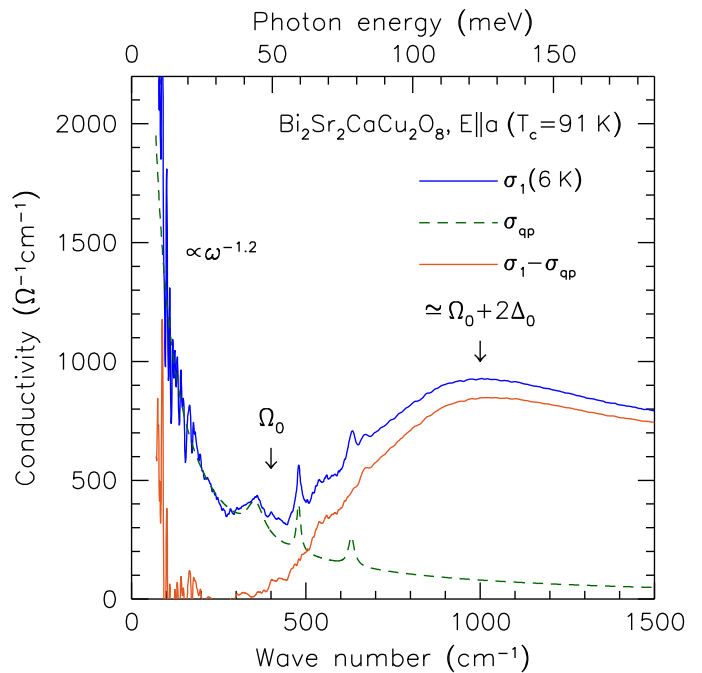


**Figure 2 | The decomposition of the optical conductivity in a cuprate superconductor.** The optical conductivity of optimally-doped  $\text{Bi}_2\text{Sr}_2\text{CaCu}_2\text{O}_{8+\delta}$  at 6 K versus wave number (photon energy) with the residual quasiparticle conductivity shown and removed; several sharp features in the conductivity have been fit to Lorentzian oscillators (Supplementary Information) and have also been removed. The subtracted spectra shows an onset of absorption at  $\Omega_0$  and a local maximum at  $\simeq \Omega_0 + 2\Delta_0$ .

layer graphene in the linear dependence of the resistivity which is the result of electron-phonon (acoustic phonon) coupling [35]. However, in the materials discussed here, the electron-phonon coupling is weak. The power-law behavior observed in this work is likely the result of the scattering of nodal quasiparticles by low-energy (bosonic) excitations, or possibly some unique self-energy effect of the Dirac-like quasiparticles. What is common for these systems are the existence of antiferromagnetic spin fluctuations (or over-damped spin density waves in the SDW materials), which may be the underlying mechanism that gives rise to the nearly linear frequency dependence of the scattering rate.

## METHODS

The temperature dependence of the absolute reflectance was measured at a near-normal angle of incidence over a wide frequency range using an *in situ* evaporation method [36]. In this study mirror-like as-grown crystal faces have been examined. The complex optical properties were determined from a Kramers-Kronig analysis of the reflectance [37]. The Kramers-Kronig

transform requires that the reflectance be determined for all frequencies, thus extrapolations must be supplied in the  $\omega \rightarrow 0, \infty$  limits. In the metallic state the low frequency extrapolation follows the Hagen-Rubens form,  $R(\omega) \propto 1 - a\sqrt{\omega}$ , while in the superconducting state  $R(\omega) \propto 1 - a\omega^4$  is typically employed; however, it should be noted that when the reflectance is close to unity the analysis is not sensitive upon the choice of low-frequency extrapolation. The reflectance is assumed to be constant above the highest measured frequency point up to  $\simeq 1 \times 10^5 \text{ cm}^{-1}$ , above which a free electron gas asymptotic reflectance extrapolation  $R(\omega) \propto 1/\omega^4$  is employed [38].

## ACKNOWLEDGMENTS

The authors would like to acknowledge useful discussions with P. W. Anderson, Y. M. Dai, D. N. Basov, D. A. Bonn, S. V. Borisenko, G. Kotliar, P. Phillips, J. D. Rameau, D. Schmeltzer and C. Varma. Research supported by the U.S. Department of Energy, Office of Basic Energy Sciences, Division of Materials Sciences and Engineering under Contract No. DE-AC02-98CH10886. C.C.H. would like to acknowledge the hospitality of the Theory Institute for Strongly Correlated and Complex Systems.

## SUPPLEMENTARY INFORMATION

### Modeling the optical conductivity of the cuprates

The interpretation of the free-carrier response in the low-frequency optical conductivity of the high-temperature superconductors has always presented a challenge due to the curious nature of the flat, essentially incoherent, mid-infrared response [8]. Two approaches have been developed to model this behavior. The first is a single-component model which considers delocalized carriers interacting strongly with an optically inactive (bosonic) excitation in which the scattering rate and the effective mass both have a strong frequency dependence [39, 40]. The second approach is a two-component model which associates the low-frequency conductivity with a free-carrier response, and the mid-infrared conductivity with one or more bound excitations [41].

Initially, we consider the two-component approach, where the optical conductivity has been fit in both the normal state by assuming that the scattering rate for the free carriers has a temperature dependence but is frequency independent,  $1/\tau(\omega, T) \simeq 1/\tau_0 + \mathcal{O}(T^2)$ . This is equivalent to the Drude model for a metal. The mid-infrared conductivity has been modeled with Lorentzian oscillators, so that the complex dielectric function  $\tilde{\epsilon} =$

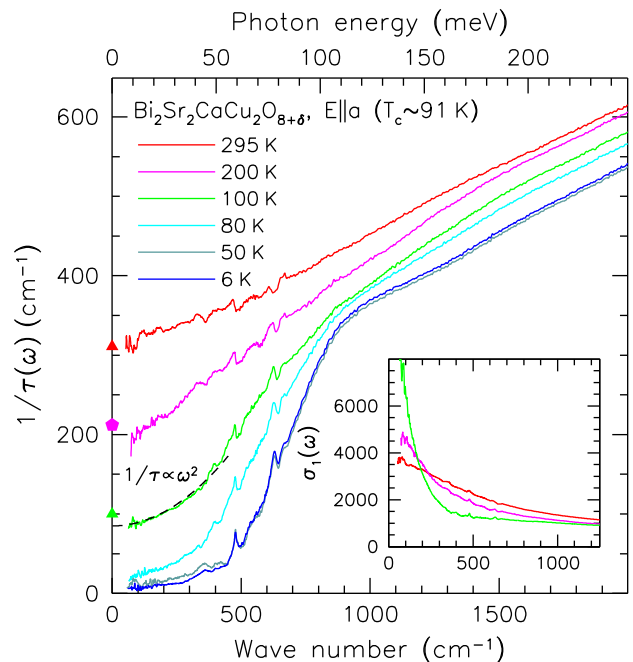


**Figure S1 | Frequency-dependent scattering rate of  $\text{Bi}_2\text{Sr}_2\text{CaCu}_2\text{O}_{8+\delta}$ .** The temperature dependence of the frequency-dependent scattering rate versus wave number (photon energy) for the cuprate superconductor  $\text{Bi}_2\text{Sr}_2\text{CaCu}_2\text{O}_{8+\delta}$  at optimal doping ( $T_c = 91 \text{ K}$ ) for light polarized in the  $a$ - $b$  planes. In the normal state, the scattering rates determined from the Drude-Lorentz fits agree well the extrapolated  $1/\tau(\omega \rightarrow 0)$  values; however, below  $T_c$  this model cannot accurately determine the scattering rates of the residual quasiparticles. Inset: the normal-state optical conductivity.

$\epsilon_1 + i\epsilon_2$  for these two contributions is the simple Drude-Lorentz model

$$\tilde{\epsilon}(\omega) = \epsilon_\infty - \frac{\omega_p^2}{\omega^2 + i\omega/\tau} + \sum_j \frac{\Omega_j^2}{\omega_j^2 - \omega^2 - i\omega\gamma_j}, \quad (1)$$

where  $\epsilon_\infty$  is the high-frequency contribution to the real part of the dielectric function,  $\omega_p^2 = 4\pi n e^2 / m_b$  and  $1/\tau$  are the square of the plasma frequency and scattering rate, respectively, and  $\omega_j$ ,  $\gamma_j$  and  $\Omega_j$  are the position, width, and oscillator strength of the  $j$ th vibration or bound excitation. The complex conductivity is  $\tilde{\sigma}(\omega) = \sigma_1 + i\sigma_2 = i\omega[\epsilon_\infty - \tilde{\epsilon}(\omega)]/4\pi$ , so that the real part of the optical conductivity is  $\sigma_1(\omega) = \omega\epsilon_2/60$  (in units of  $\Omega^{-1}\text{cm}^{-1}$ ). The Drude-Lorentz model has been fit to the real part of the optical conductivity using a non-linear least-squares method. The result for the fit to optimally-doped  $\text{Bi}_2\text{Sr}_2\text{CaCu}_2\text{O}_{8+\delta}$  ( $T_c = 91 \text{ K}$ ) for light polarized along the  $a$  axis in the normal state at 100 K yields  $\omega_p \simeq 8560 \text{ cm}^{-1}$  and  $1/\tau \simeq 100 \text{ cm}^{-1}$ . The agreement with experiment is quite good, but it should be noted that the number and location of the Lorentzian oscillators required to achieve this fit is somewhat ar-

bitrary. The presence of these mid-infrared oscillators is difficult to physically justify given that the cuprates typically only have a single band crossing the Fermi surface [13], with no other features nearby that would readily account for these excitations. This suggests that we should instead consider a single channel, or single component, for the conductivity in which the charge carriers are strongly renormalized.

The single-component model considers the simple Drude model for an uncorrelated metal, and introduces a frequency dependence into the scattering rate and effective mass,

$$\tilde{\epsilon}(\omega) = \epsilon_\infty - \frac{\omega_p^2}{[m^*(\omega)/m_b][\omega^2 + i\omega/\tau(\omega)]}. \quad (2)$$

The frequency-dependent scattering rate and mass enhancement factor may then be determined experimentally [39, 40]:

$$\frac{1}{\tau(\omega)} = \frac{\omega_p^2}{4\pi} \text{Re} \left[ \frac{1}{\tilde{\sigma}(\omega)} \right] \quad (3)$$

and

$$\frac{m^*(\omega)}{m_b} = \frac{\omega_p^2}{4\pi} \frac{1}{\omega} \text{Im} \left[ \frac{1}{\tilde{\sigma}(\omega)} \right], \quad (4)$$

where  $m_b$  is the band mass,  $m^*(\omega)/m_b = 1 + \lambda(\omega)$ , and  $\lambda(\omega)$  is a frequency-dependent electron-boson coupling constant. The temperature dependence of the frequency-dependent scattering rate for optimally-doped  $\text{Bi}_2\text{Sr}_2\text{CaCu}_2\text{O}_{8+\delta}$  is shown in Fig. S1 using the previously determined value for  $\omega_p$  in the normal state. Aside from  $1/\tau(\omega)$  being somewhat smaller due to our choice of  $\omega_p$ , it is consistent with other results [42]. The polygons denote the values for  $1/\tau$  returned from the Drude-Lorentz fits. In general, we would expect the fitted values for  $1/\tau$  from the Drude-Lorentz model to agree with  $1/\tau(\omega \rightarrow 0)$  in the normal state, and this is indeed the case. At room temperature  $1/\tau(\omega)$  is roughly linear in frequency, and therefore consistent with a marginal Fermi liquid [43, 44]. As the temperature is lowered the scattering rate develops a quadratic component just above  $T_c$  up to  $\simeq 400 \text{ cm}^{-1}$ , above which the scattering rate increases dramatically, as reflected by the kink in the optical conductivity at 100 K shown in the inset of Fig. S1. This suggests that just above  $T_c$  the transport in the normal state may be cautiously described as a Fermi liquid; this is in agreement with the proposed phase diagram of the high-temperature cuprate superconductors [10]. Interestingly, a similar quadratic frequency dependence in  $1/\tau(\omega)$  has also been observed in the normal state of the strongly underdoped single-layer cuprate material  $\text{HgBa}_2\text{CuO}_{4+\delta}$  ( $T_c = 67 \text{ K}$ ) and interpreted as evidence of Fermi-liquid like behavior [24], indicating that the underdoped region of the cuprates is still a rapidly evolving area.

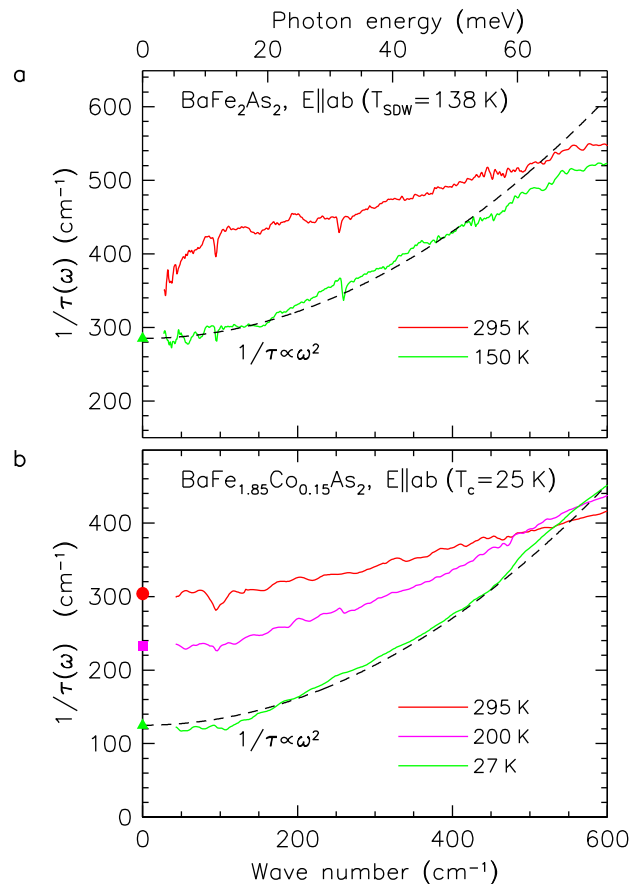


**Figure S2 | Frequency-dependent scattering rate in iron-based materials.** **a**, The temperature dependence of the frequency-dependent scattering rate versus wave number (photon energy) for  $\text{BaFe}_2\text{As}_2$  for  $T > T_{\text{SDW}}$ . **b**, The temperature dependence of the frequency-dependent scattering rate versus wave number (photon energy) for  $\text{BaFe}_{1.85}\text{Co}_{0.15}\text{As}_2$  for  $T > T_c$ . In both cases a curve with a quadratic frequency dependence has been superimposed on the low-temperature data.

Below  $T_c$  the picture is considerably more complicated. While the collapse of the low-frequency scattering rate is consistent with the collapse of the quasiparticle scattering rate observed in the microwave experiments [17], it is in fact due to the formation of a condensate that dominates the imaginary part of the optical conductivity,  $\sigma_2$ . Adopting a simple two-fluid model for the behavior of the superconducting state [45], it may be shown that for  $T \ll T_c$ , the condition  $\sigma_1 \ll \sigma_2$  is satisfied; given  $1/\tau(\omega) \propto \sigma_1/(\sigma_1^2 + \sigma_2^2)$ , then to leading order  $1/\tau(\omega) \propto \sigma_1/\sigma_2^2$ , indicating that below  $T_c$  the scattering rate is dominated by the formation of a superconducting condensate. Therefore, in the superconducting state this approach may not be used to make any reliable statements about the scattering rate of the unpaired quasiparticles responsible for the residual conductivity. The small values for  $1/\tau$  for  $T < T_c$  determined from

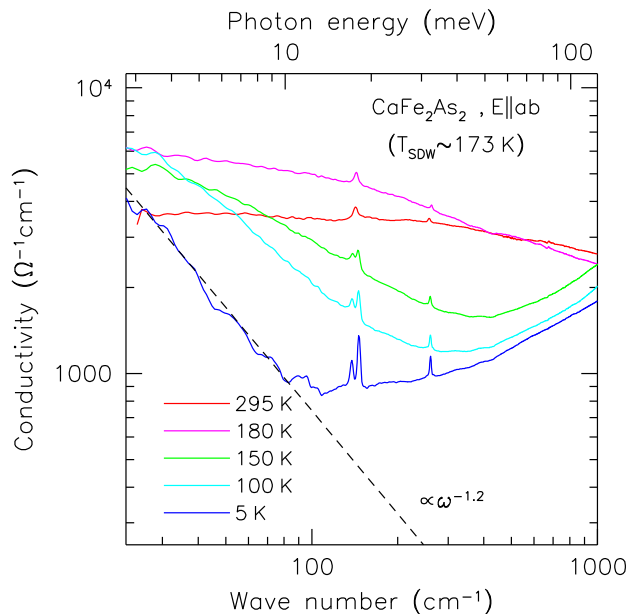


**Figure S3 | Fractional power law in the optical conductivity of  $\text{CaFe}_2\text{As}_2$ .** The log-log plot of the temperature dependence of the real part of the optical conductivity versus wave number (photon energy) for the iron-based material  $\text{CaFe}_2\text{As}_2$  ( $T_{\text{SDW}} \simeq 173$  K) for light polarized in the  $a$ - $b$  planes. The low-frequency data at 6 K displays a  $\sigma_1 \propto \omega^{-1.2}$  dependence.

microwave studies indicate that we are in the  $\omega\tau \gg 1$  regime, so that if the unpaired quasiparticles constitute a Fermi liquid then  $\sigma_1 \propto \omega^{-2}$  behavior should be recovered; however, we instead observe the fractional power law  $\sigma_1 \propto \omega^{-1.2}$ . This indicates that while the carriers just above  $T_c$  in the normal state might be described as a Fermi liquid, the optical properties of the residual conductivity below  $T_c$  describe a non-Fermi liquid. (We note that as  $\omega \rightarrow 0$  we will eventually recover  $\omega\tau \sim 1$ , at which point we would expect a roll-off in the conductivity as it becomes largely frequency independent.)

In summary, the one and two-component models both provide useful information about the normal and superconducting states. However, in the Drude-Lorentz picture the low-frequency Lorentzian oscillators required to obtain a reasonable fit to the optical conductivity do not have a clear physical origin, and it is likely that this is the result of the two-component model being forced to deal with a strongly renormalized free-carrier scattering rate. This suggests that at low frequencies the single component model is a better description of the delocalized carriers, which in the normal state close to  $T_c$ , may be cautiously described as a Fermi liquid.

## $\text{BaFe}_2\text{As}_2$ and $\text{BaFe}_{1.85}\text{Co}_{0.15}\text{As}_2$

The pnictide materials are multiband systems [25] that have been modeled using a two-Drude approach [46] to describe the hole and electron pockets. However, in some of these materials it may be argued that a single band dominates the transport properties; the assumption of a single band allows the cautious application of the generalized Drude model. The frequency dependent scattering rate of the pnictide  $\text{BaFe}_2\text{As}_2$  ( $T_{\text{SDW}} = 138$  K) develops a clear quadratic frequency dependence in the non-magnetic state for  $T \gtrsim T_{\text{SDW}}$ , shown in Fig. S2a, suggesting that this material may be described as a Fermi liquid. Interestingly, when the magnetic and structural transition in this material is suppressed through Co substitution in  $\text{BaFe}_{1.85}\text{Co}_{0.15}\text{As}_2$  and superconductivity is induced ( $T_c = 25$  K), the quadratic behavior is observed in the normal state at low temperature,  $T \gtrsim T_c$ , shown in Fig. S2b.

## $\text{CaFe}_2\text{As}_2$

The iron-arsenic  $\text{CaFe}_2\text{As}_2$  material is similar to  $\text{BaFe}_2\text{As}_2$ , having a spin-density-wave (SDW) transition at  $T_{\text{SDW}} \simeq 173$  K, below which it remains metallic. The non-Fermi liquid power law behavior observed in the low-frequency optical conductivity in the ground state of the cuprate materials and  $\text{BaFe}_2\text{As}_2$ ,  $\sigma_1 \propto \omega^{-1.2}$ , is also observed in  $\text{CaFe}_2\text{As}_2$  material well below  $T_{\text{SDW}}$ , as shown in Fig. S3.

## Decomposition of the optical conductivity of $\text{YBa}_2\text{Cu}_3\text{O}_{6+y}$

The sharp structures in the conductivity in optimally-doped  $\text{YBa}_2\text{Cu}_3\text{O}_{6.95}$ , shown in Fig. S4a, and in underdoped  $\text{YBa}_2\text{Cu}_3\text{O}_{6.60}$ , shown in Fig. S4b, for light polarized along the crystallographic  $a$  axis are attributed to the normally infrared-active  $B_{3u}$  modes [47], which have been fit to the data using Lorentzian oscillators (described earlier), in linear combination with a polynomial background. The oscillators are added to the fractional power law expression for the conductivity for the unpaired quasiparticles below  $T_c$  and subtracted from the optical conductivity. In both cases a value of  $\Omega_0 \simeq 50$  meV is obtained, which is once again consistent with inversion methods [34]. In the optimally-doped material, the estimate of  $\Delta_0 \simeq 30$  meV is similar to what is obtained in tunneling studies [48]. However, in the underdoped data there is a considerable amount of structure at low frequency and there is no longer an obvious feature that can be identified with the gap maximum.

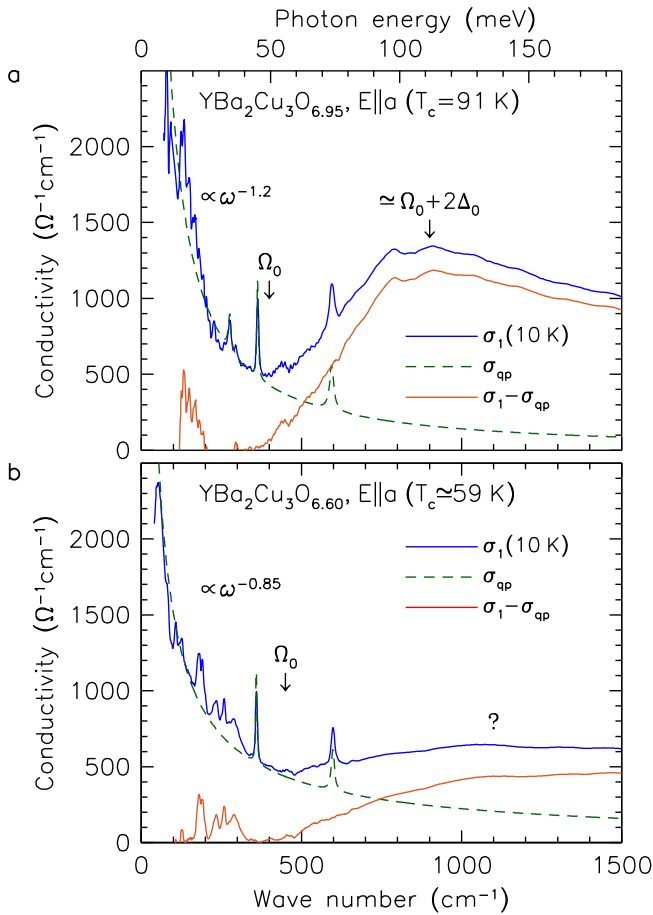


**Figure S4** | The decomposition of the optical conductivity of  $\text{YBa}_2\text{Cu}_3\text{O}_{6+y}$ . **a**, The optical conductivity of optimally-doped  $\text{YBa}_2\text{Cu}_3\text{O}_{6.95}$  versus wave number (photon energy) at 10 K with the residual quasiparticle conductivity removed; the subtracted spectra shows an onset of absorption at  $\Omega_0$  and a local maximum at  $\Omega_0 + 2\Delta_0$ . **b**, Underdoped  $\text{YBa}_2\text{Cu}_3\text{O}_{6.60}$  at 10 K.

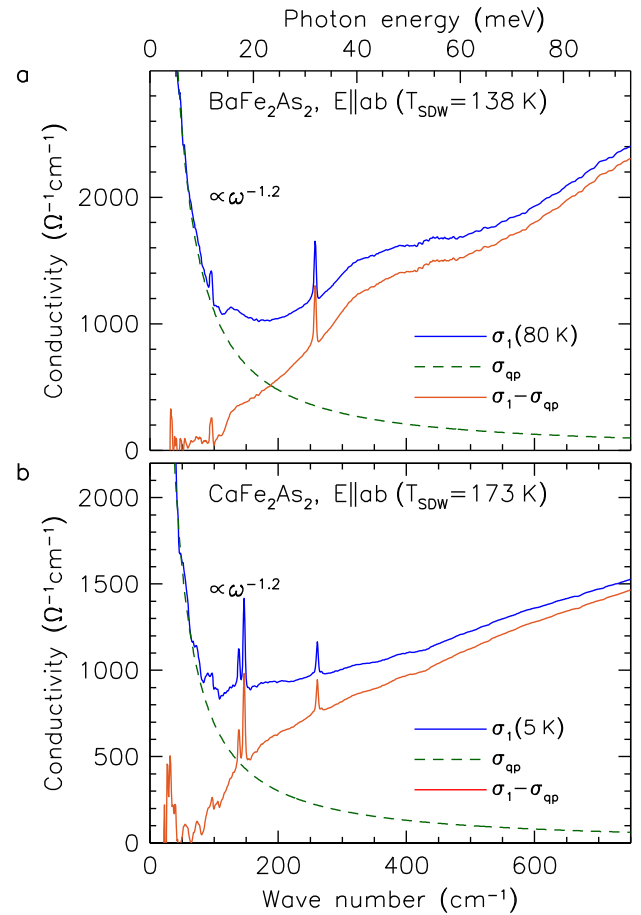


**Figure S5** | The decomposition of the optical conductivity in iron-based materials. **a**, The optical conductivity of  $\text{BaFe}_2\text{As}_2$  versus wave number (photon energy) at 80 K with the residual quasiparticle conductivity removed showing the onset of absorption at  $\omega \gtrsim 0$ . **b**,  $\text{CaFe}_2\text{As}_2$  at 5 K.

### Decomposition of the optical conductivity of $\text{BaFe}_2\text{As}_2$ and $\text{CaFe}_2\text{As}_2$

In the iron-pnictide materials, the metallic compounds  $\text{BaFe}_2\text{As}_2$  and  $\text{CaFe}_2\text{As}_2$  have magnetic and structural transitions at  $T_{\text{SDW}} = 138$  and  $173$  K, respectively, below which they remain metallic [25]. Below  $T_{\text{SDW}}$  the Fermi surface undergoes a reconstruction and a Dirac-cone like gap opens in the electronic dispersion at (or close to) the Fermi level [27, 49]. In  $\text{BaFe}_2\text{As}_2$  at 80 K, and  $\text{CaFe}_2\text{As}_2$  at 5 K, the low-frequency conductivity is described quite well by the fractional power law  $\sigma_1 \propto \omega^{-1.2}$ . The residual conductivity has been subtracted from the optical conductivity in these materials in Fig. S5 revealing that, unlike the cuprate superconductors surveyed where the onset of absorption does not begin until  $\sim \Omega_0$ , the absorption commences at a much lower frequency,  $\omega \gtrsim 0$ .

\* homes@bnl.gov

† jtu@sci.ccny.cuny.edu

- [1] R. N. Gurzhi, Soviet Physics JETP **20**, 953 (1965).
- [2] U. Nagel, T. Uleksin, T. Rm, R. P. S. M. Lobo, P. Lejay, C. C. Homes, J. S. Hall, A. W. Kinross, S. K. Purdy, T. Munsie, T. J. Williams, G. M. Luke, and T. Timusk, PNAS **109**, 19161 (2012).
- [3] D. van der Marel, Phys. Rev. B **60**, R765 (1999).
- [4] J. S. Dodge, C. P. Weber, J. Corson, J. Orenstein, Z. Schlesinger, J. W. Reiner, and M. R. Beasley, Phys. Rev. Lett. **85**, 4932 (2000).
- [5] J. Orenstein and A. J. Millis, Science **288**, 468 (2000).
- [6] S. V. Dordevic and D. N. Basov, Ann. Phys. **15**, 545 (2006).
- [7] C. Berthod, J. Mravlje, X. Deng, R. Žitko, D. van der Marel, and A. Georges, Phys. Rev. B **87**, 115109 (2013).
- [8] D. N. Basov and T. Timusk, Rev. Mod. Phys. **77**, 721 (2005).

- [9] J. J. Tu, C. C. Homes, G. D. Gu, D. N. Basov, and M. Strongin, *Phys. Rev. B* **66**, 144514 (2002).
- [10] D. M. Broun, *Nat. Phys.* **4**, 170 (2008).
- [11] R. G. Buckley, H. S. Barowski, and K. F. Renk, *Phys. Rev. B* **64**, 014509 (2001).
- [12] D. J. Van Harlingen, *Rev. Mod. Phys.* **67**, 515 (1995).
- [13] A. Damascelli, Z. Hussain, and Z.-X. Shen, *Rev. Mod. Phys.* **75**, 473 (2003).
- [14] P. A. Lee, *Phys. Rev. Lett.* **71**, 1887 (1993).
- [15] A. K. Geim and K. S. Novoselov, *Nat. Mater.* **6**, 183 (2007).
- [16] J. E. Moore, *Nature* **464**, 194 (2010).
- [17] T. Shibauchi, H. Kitano, A. Maeda, H. Asaoka, H. Takei, I. Shigaki, T. Kimura, K. Kishio, K. Izumi, T. Suzuki, and K. Uchinokura, *J. Phys. Soc. Jpn.* **65**, 3266 (1996).
- [18] C. C. Homes, D. A. Bonn, R. Liang, W. N. Hardy, D. N. Basov, T. Timusk, and B. P. Clayman, *Phys. Rev. B* **60**, 9782 (1999).
- [19] T. Timusk and B. Statt, *Rep. Prog. Phys.* **62**, 61 (1999).
- [20] Y. Ando, A. N. Lavrov, S. Komiya, K. Segawa, and X. F. Sun, *Phys. Rev. Lett.* **87**, 017001 (2001).
- [21] Y. S. Lee, K. Segawa, Z. Q. Li, W. J. Padilla, M. Dumm, S. V. Dordevic, C. C. Homes, Y. Ando, and D. N. Basov, *Phys. Rev. B* **72**, 054529 (2005).
- [22] A. Kanigel, M. R. Norman, M. Randeria, U. Chatterjee, S. Souma, A. Kaminski, H. M. Fretwell, S. Rosenkranz, M. Shi, T. Sato, T. Takahashi, Z. Z. Li, H. Raffy, K. Kadowaki, D. Hinks, L. Ozyuzer, and J. C. Campuzano, *Nature Phys.* **2**, 447 (2006).
- [23] P. J. Turner, R. Harris, S. Kamal, M. E. Hayden, D. M. Broun, D. C. Morgan, A. Hosseini, P. Dosanjh, G. K. Mullins, J. S. Preston, R. Liang, D. A. Bonn, and W. N. Hardy, *Phys. Rev. Lett.* **90**, 237005 (2003).
- [24] S. I. Mirzaei, D. Stricker, J. N. Hancock, C. Berthod, A. Georges, E. van Heumen, M. K. Chan, X. Zhao, Y. Li, M. Greven, N. Barišić, and D. van der Marel, *PNAS* **110**, 5774 (2013).
- [25] D. C. Johnston, *Adv. Phys.* **59**, 803 (2010).
- [26] V. B. Zabolotnyy, D. S. Inosov, D. V. Evtushinsky, A. Koitzsch, A. A. Kordyuk, G. L. Sun, J. T. Park, D. Haug, V. Hinkov, A. V. Boris, C. T. Lin, M. Knupfer, A. N. Yaresko, B. Buchner, A. Varykhalov, R. Follath, and S. V. Borisenko, *Nature* **457**, 569 (2009).
- [27] P. Richard, K. Nakayama, T. Sato, M. Neupane, Y.-M. Xu, J. H. Bowen, G. F. Chen, J. L. Luo, N. L. Wang, X. Dai, Z. Fang, H. Ding, and T. Takahashi, *Phys. Rev. Lett.* **104**, 137001 (2010).
- [28] W. Z. Hu, J. Dong, G. Li, Z. Li, P. Zheng, G. F. Chen, J. L. Luo, and N. L. Wang, *Phys. Rev. Lett.* **101**, 257005 (2008).
- [29] W. A. Harrison, *Solid State Theory* (McGraw-Hill, New York, 1970) p. 320.
- [30] R. Akis, J. P. Carbotte, and T. Timusk, *Phys. Rev. B* **43**, 12804 (1991).
- [31] E. J. Nicol, J. P. Carbotte, and T. Timusk, *Phys. Rev. B* **43**, 473 (1991).
- [32] J. P. Carbotte, E. Schachinger, and D. N. Basov, *Nature* **401**, 354 (1999).
- [33] D. Munzar, C. Bernhard, and M. Cardona, *Physica C* **312**, 121 (1999).
- [34] S. V. Dordevic, C. C. Homes, J. J. Tu, T. Valla, M. Strongin, P. D. Johnson, G. D. Gu, and D. N. Basov, *Phys. Rev. B* **71**, 104529 (2005).
- [35] K. I. Bolotin, K. J. Sikes, J. Hone, H. L. Stormer, and P. Kim, *Phys. Rev. Lett.* **101**, 096802 (2008).
- [36] C. C. Homes, M. Reedyk, D. A. Crandles, and T. Timusk, *Appl. Opt.* **32**, 2976 (1993).
- [37] M. Dressel and G. Grüner, *Electrodynamics of Solids* (Cambridge University Press, Cambridge, 2001).
- [38] F. Wooten, *Optical Properties of Solids* (Academic Press, New York, 1972) pp. 244–250.
- [39] J. W. Allen and J. C. Mikkelsen, *Phys. Rev. B* **15**, 2952 (1977).
- [40] A. V. Puchkov, D. N. Basov, and T. Timusk, *J. Phys.: Condens. Matter* **8**, 10049 (1996).
- [41] D. B. Tanner and T. Timusk, in *Physical Properties of High-Temperature Superconductors III*, edited by D. N. Ginsberg (World Scientific, Singapore, 1992) pp. 363–469.
- [42] J. Hwang, T. Timusk, and G. D. Gu, *J. Phys.: Condens. Matter* **19**, 125208 (2007).
- [43] P. B. Littlewood and C. M. Varma, *J. Appl. Phys.* **69**, 4979 (1991).
- [44] J. Hwang, T. Timusk, A. V. Puchkov, N. L. Wang, G. D. Gu, C. C. Homes, J. J. Tu, and H. Eisaki, *Phys. Rev. B* **69**, 094520 (2004).
- [45] D. A. Bonn, R. Liang, T. M. Riseman, D. J. Baar, D. C. Morgan, K. Zhang, P. Dosanjh, T. L. Duty, A. MacFarlane, G. D. Morris, J. H. Brewer, W. N. Hardy, C. Kallin, and A. J. Berlinsky, *Phys. Rev. B* **47**, 11314 (1993).
- [46] D. Wu, N. Barišić, P. Kallina, A. Faridian, B. Gorshunov, N. Drichko, L. J. Li, X. Lin, G. H. Cao, Z. A. Xu, N. L. Wang, and M. Dressel, *Phys. Rev. B* **81**, 100512 (2010).
- [47] C. C. Homes, A. W. McConnell, B. P. Clayman, D. A. Bonn, R. Liang, W. N. Hardy, M. Inoue, H. Negishi, P. Fournier, and R. L. Greene, *Phys. Rev. Lett.* **84**, 5391 (2000).
- [48] N.-C. Yeh, C.-T. Chen, G. Hammerl, J. Mannhart, A. Schmehl, C. W. Schneider, R. R. Schulz, S. Tajima, K. Yoshida, D. Garrigus, and M. Strasik, *Phys. Rev. Lett.* **87**, 087003 (2001).
- [49] S. Sugai, Y. Mizuno, R. Watanabe, T. Kawaguchi, K. Takenaka, H. Ikuta, Y. Takayanagi, N. Hayamizu, and Y. Sone, *J. Phys. Soc. Jpn.* **81**, 024718 (2012).